Polyhedron 28 (2009) 3797–3803

Contents lists available at ScienceDirect

Polyhedron

journal homepage: www.elsevier.com/locate/poly

Copper(II) and zinc(II) complexes with 2-formylpyridine-derived hydrazones

Angel A. Recio Despaigne [a], Jeferson G. da Silva [a], Ana Cerúlia M. do Carmo [a], Flavio Sives [b], Oscar E. Piro [b], Eduardo E. Castellano [c], Heloisa Beraldo [a,*]

[a] Departamento de Química, Universidade Federal de Minas Gerais 31270-901, Belo Horizonte, MG, Brazil
[b] Departamento de Física, Facultad de Ciencias Exactas, Universidad Nacional de La Plata and Instituto IFLP (CONICET, CCT-La Plata), C.C. 67, 1900 La Plata, Argentina
[c] Instituto de Física de São Carlos, Universidade de São Paulo, C.P. 369, 13560-970 São Carlos (SP), Brazil

ARTICLE INFO

Article history:
Received 31 January 2009
Accepted 31 July 2009
Available online 7 August 2009

Keywords:
Hydrazones
Metal complexes
Crystal structure

ABSTRACT

In the present work 2-formylpyridine-*para*-chloro-phenyl hydrazone (H2FopClPh) and 2-formylpyridine-*para*-nitro-phenyl hydrazone ($H2FopNO_2Ph$) were obtained, as well as their copper(II) and zinc(II) complexes $[Cu(H2FopClPh)Cl_2]$ (**1**), $[Cu(2FopNO_2Ph)Cl]$ (**2**), $[Zn(H2FopClPh)Cl_2]$ (**3**) and $[Zn(H2FopNO_2Ph)Cl_2]$ (**4**). Upon re-crystallization in DMSO:acetone conversion of **2** into $[Cu(2FopNO_2Ph)Cl(DMSO)]$ (**2a**) and of **4** into $[Zn(2FopNO_2Ph)Cl(DMSO)]$ (**4a**) occurred. The crystal structures of **1**, **2a**, **3** and **4a** were determined.

1. Introduction

Hydrazones are an important class of compounds which present innumerous pharmacological applications as antimicrobial, anticonvulsant, analgesic, antiinflammatory, antiplatelet, antitubercular, and antitumoral agents [1–3].

Metal complexes of hydrazones proved to have potential applications as catalysts [4], luminescent probes [5], and molecular sensors [6]. Moreover, it has been recently shown that hydrazones such as pyridoxal isonicotinoyl hydrazone (PIH) analogs are effective iron chelators *in vivo* and *in vitro*, and may be of value for the treatment of iron overload [7].

In the present work 2-formylpyridine-*para*-chloro-phenyl hydrazone (H2FopClPh) and 2-formylpyridine-*para*-nitro-phenyl hydrazone ($H2FopNO_2Ph$) were obtained as well as their copper(II) and zinc(II) complexes. The spectral and structural properties of the complexes were investigated (see structural representation of the hydrazones in Fig. 1).

2. Experimental

2.1. Materials and equipment

Partial elemental analyses were performed on a Perkin–Elmer CHN 2400 analyzer. Infrared spectra were recorded on a Perkin–Elmer FT-IR Spectrum GX spectrometer using CsI/nujol; an YSI model 31 conductivity bridge was employed for molar conductivity measurements. Electronic spectra were acquired with a Hewlett–Packard 8453 spectrometer in dimethyl formamide (DMF) solutions using 1 cm cells. Magnetic susceptibility measurements were carried out at room temperature on a Johnson Matthey MSB/AUTO balance and as a function of temperature in a Lake-Shore 7130 susceptometer with an a.c. excitation field of 1 Oe in amplitude and a frequency of 825 Hz at null static magnetic field. NMR spectra were obtained at room temperature with a Brucker DRX-400 Avance (400 MHz) spectrometer using deuterated dimethyl sulfoxide (DMSO-d_6) as the solvent and tetramethylsilane (TMS) as internal reference.

The molecular structures of the copper(II) and zinc(II) complexes were investigated using single-crystal X-ray diffractometry. The measurements were performed on an Enraf-Nonius Kappa-CCD diffractometer with graphite-monochromated Mo Kα ($\lambda = 0.71073$ Å) radiation. Diffraction data were collected (φ and ω scans with κ-offsets) with COLLECT [8]. Integration and scaling of the reflections were performed with HKL DENZO-SCALEPACK suite of programs. The unit cell parameters were obtained by least-squares refinement based on the angular settings for all collected reflections using HKL SCALEPACK [9]. The data were corrected numerically for absorption with PLATON [10]. The structures were solved by direct methods with SHELXS-97 [11] and the molecular model refined by full-matrix least-squares procedure on F^2 with SHELXL-97 [12]. The crystallization DMSO solvent of **1** (and to a much less degree also **3**) showed positional disorder which was modeled in terms of a two-split molecules refined such as their site

* Corresponding author. Tel.: +55 31 3499 5740; fax: +55 31 3499 5700.
E-mail address: hberaldo@ufmg.br (H. Beraldo).

0277-5387/$ - see front matter © 2009 Elsevier Ltd. All rights reserved.
doi:10.1016/j.poly.2009.07.059

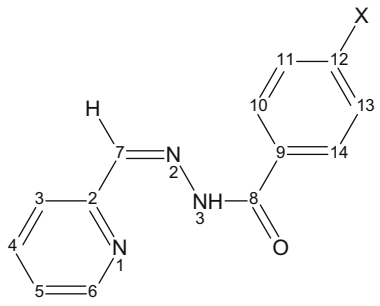

X = Cl (for H2FopClPh) or NO_2 (for H2FopNO_2Ph)

Fig. 1. Structural representation for 2-formylpyridine-*para*-chloro-phenyl hydrazone (H2FopClPh) and 2-formylpyridine-*para*-nitro-phenyl hydrazone (H2FopNO_2Ph).

occupancy factors summed up to one. The hydrogen atoms of the hydrazones were included in the molecular models at stereochemical positions and refined with the riding model. The DMSO ligand methyl H-atoms of complexes **2a** and **4a** were optimized by treating them as a rigid group which was allowed to rotate around the corresponding C–S bond. A similar treatment was given to the CH_3 groups of the crystallization DMSO of **3**. Crystal data and refinement results are summarized in Tables 1a and b.

2.2. Syntheses of 2-formylpyridine-para-chloro-phenyl hydrazone (H2FopClPh) and 2-formylpyridine-para-nitro-phenyl hydrazone (H2FopNO_2Ph)

The hydrazones were prepared by mixing equimolar (1 mmol) amounts of 2-formylpyridine with the desired hydrazide in methanol with addition of three drops of acetic acid as catalyst. The reaction mixture was kept under reflux for 6 h. After cooling to room temperature the resulting solids were filtered off, washed with ethanol and ether and dried *in vaccuo*.

2.2.1. 2-Formylpyridine-para-chloro-phenyl hydrazone (H2FopClPh)

Color: White. Yield: 76% M.P: 166.3–167.9 °C. Selected IR Bands (cm^{-1}): υ(NH) 3175 m; υ(C=O) 1651 s; υ(C=N) 1592 m; ρ(py) 618 m. UV–Vis (DMF, cm^{-1}): 33 110. ^{1}H NMR [400 MHz, DMSO-d_6, δ (ppm)]: 12.15 (s, 1H, NH); 8.65 (d, 1H, H6); 8.51 (s, 1H, H7); 8.01 (d, 1H, H3); 7.97 [d, 2H, H(10,14)]; 7.91 (t, 1H, H4); 7.66 [d, 2H, H(11,13)]; 7.44 (t, 1H, H5). ^{13}C NMR [400 MHz, DMSO-d_6, δ (ppm)]: 162.3 (C8); 153.2 (C2); 149.6 (C6); 148.4 (C7); 136.9 (C4); 131.9 (C9); 129.7 [C(10,14)]; 128.7 [C(11,13)]; 124.5 (C5); 120.0 (C3).

2.2.2. 2-Formylpyridine-para-nitro-phenyl hydrazone mono hydrate [H2FopNO_2Ph]$_2$·2H_2O

Color: Beige Yield: 87% M.P: 218–220 °C. Selected IR Bands (cm^{-1}): =υ(NH) 3227 m; υ(C=O) 1664 s; υ(C=N) 1601 m; ρ(py) 619 m. UV–Vis (DMF, cm^{-1}): 32 890. ^{1}H NMR [400 MHz, DMSO-d_6, δ (ppm)]: 15.83(*Z*), 12.33(*E*) [s, 1H, NH(*Z* and *E* isomers)]; 8.92 (*Z*), 8.64 (*E*) [d,1H, H6(*Z* and *E* isomers)]; 8.31–8.52 (*Z*,*E*) [m, 1H, H3(*Z* and *E* isomers)]; 8.49 (*E*) [s, 1H, H7(*E* isomers)]; 8.39 (*E*) [d, 2H, H(11,13) (*E* isomers)]; 8.17 [d, 2H, H(10,14) (*E* isomers)]; 7.99(*Z*), 7.87(*E*) [t, 1H, H4(*Z* and *E* isomers)]; 7.63(*Z*), 7.45(*E*) [t, 1H, H5 (*Z* and *E* isomers)]. ^{13}C NMR [400 MHz, DMSO-d_6, δ (ppm)]: 182.9 (*Z*), 161.8 (*E*) [C8 (*Z* and *E* isomers)]; 153.0 (*E*) [C2(*E* isomer)]; 149.6 (*Z*), 149.2 (*E*) [C6 (*Z* and *E* isomers)]; 149.4 (*E*) [C7 (*E* isomer)]; 148.5 (*E*) [C12 (*E* isomer)]; 138.8 (*Z*), 137.0 (*E*) [C4 (*Z* and *E* isomers)]; 128.8 (*Z*), 129.3 (*E*) [C(10,14)(*Z* and *E* isomers)]; 124.8(*E*) [C5 (*E* isomer)]; 124.7 (Z), 123.8 (*E*) [C(11,13) (*Z* and *E* isomers)]; 120.1(*E*) [C3 (*E* isomer)].

2.3. Syntheses of the zinc(II) and copper(II) complexes with H2FopClPh and H2FopNO_2Ph

The zinc(II) and copper(II) complexes (**1**–**4**) were obtained by refluxing an ethanol solution of the desired ligand with the metal chloride ($ZnCl_2$ or $CuCl_2$·2H_2O) in 1:1 ligand-to-metal molar ratio (1 mmol). The solids were washed with ethanol followed by diethylether and then dried *in vacuo*.

Table 1a
Crystal data and structure refinement results for [Cu(H2FopClPh)Cl_2] (**1**) and [Cu(2FopNO_2Ph)Cl(DMSO)] (**2a**).

	(**1**)	(**2a**)
Empirical formula	$C_{15}H_{14}Cl_3CuN_3O_2S$	$C_{15}H_{15}ClCuN_4O_4S$
Formula weight	470.24	446.36
Temperature (K)	296(2)	296(2)
Wavelength (Å)	0.71073	0.71073
Crystal system, space group	monoclinic, $P2_1/c$	monoclinic, $P2_1/n$
Unit cell dimensions		
a (Å)	8.4375(3)	9.4069(3)
b (Å)	11.9811(3)	8.1714(3)
c (Å)	18.5793(6)	23.7042(9)
β (°)	94.219(1)	91.782(2)
Volume (Å^3)	1873.1(1)	1821.2(1)
Z, calculated density (Mg/m^3)	4, 1.668	4, 1.628 Mg/m^3
Absorption coefficient (mm^{-1})	1.719	1.489
F(0 0 0)	948	908
Crystal size (mm^3)	0.16 × 0.13 × 0.05	0.20 × 0.11 × 0.04
Crystal color/shape	yellow/prism	yellow/plate
θ range for data collection	2.96–26.00°	2.64–26.00°
Index ranges	$-10 \leqslant h \leqslant 10$, $-14 \leqslant k \leqslant 14$, $-22 \leqslant l \leqslant 22$	$-11 \leqslant h \leqslant 11$, $-9 \leqslant k \leqslant 10$, $-28 \leqslant l \leqslant 29$
Reflections collected/unique [R_{int} = 0.0618]	20 540/3675 [R_{int} = 0.0598]	14 912/3565
Observed reflections [$I > 2\sigma(I)$]	3004	2771
Completeness	99.8% (to θ = 26.00°)	99.6% (to θ = 26.00°)
Refinement method	Full-matrix least-squares on F^2	Full-matrix least-squares on F^2
Data/restraints/parameters	3675/0/245	3565/0/237
Goodness-of-fit on F^2	1.056	1.080
Weights, w	$[\sigma^2(F_o^2) + (0.048P)^2 + 1.49P]^{-1}$ $P = [\mathrm{Max}(F_o^2,0) + 2F_c^2]/3$	$[\sigma^2(F_o^2) + (0.0472P)^2 + 0.39P]^{-1}$
Final *R* indices[a] [$I > 2\sigma(I)$]	R_1 = 0.0352, wR_2 = 0.0922	R_1 = 0.0372, wR_2 = 0.0875
R indices (all data)	R_1 = 0.0466, wR_2 = 0.0983	R_1 = 0.0550, wR_2 = 0.0962
Largest difference in peak and hole (e Å^{-3})	0.524 and −0.501	0.299 and −0.512

[a] $R_1 = \Sigma||F_o|-|F_c||/\Sigma|F_o|$, $wR_2 = [\Sigma w(|F_o|^2-|F_c|^2)^2/\Sigma w(|F_o|^2)^2]^{1/2}$.

Table 1b
Crystal data and structure refinement results for [Zn(H2FopClPh)Cl_2] (**3**) and [Zn(2FopNO_2Ph)Cl(DMSO)] (**4a**).

	(**3**)	(**4a**)
Empirical formula	$C_{15}H_{16}Cl_3N_3O_2SZn$	$C_{15}H_{15}ClN_4O_4$ SZn
Formula weight	474.09	448.19
Temperature (K)	296(2)	296(2)
Wavelength (Å)	0.71073	0.71073
Crystal system, space group	monoclinic, $P2_1/c$	triclinic, $P\bar{1}$
Unit cell dimensions		
a (Å)	9.6792(3)	7.9935(3)
b (Å)	10.8687(4)	9.7127(3)
c (Å)	18.8839(5)	12.1858(4)
α (°)		71.688(2)
β (°)	99.397(2)	88.947(2)
γ (°)		84.009(2)
Volume (Å^3)	1959.9(1)	893.17(5)
Z, calculated density (Mg/m^3)	4, 1.607	2, 1.667
Absorption coefficient (mm^{-1})	1.782	1.671
F(0 0 0)	960	456
Crystal size (mm^3)	0.26 × 0.22 × 0.12	0.25 × 0.12 × 0.06
Crystal color/shape	colorless/polyhedral	yellow/prism
θ Range for data collection	3.17–26.00°	3.09–26.00°
Index ranges	$-11 \leqslant h \leqslant 11$, $-13 \leqslant k \leqslant 12$, $-21 \leqslant l \leqslant 23$	$-9 \leqslant h \leqslant 9$, $-11 \leqslant k \leqslant 11$, $-15 \leqslant l \leqslant 15$
Reflections collected/unique	16 239/3829 [R_{int} = 0.0392]	10 777/3482 [R_{int} = 0.0340]
Observed reflections [$I > 2\sigma(I)$]	3210	3012
Completeness	99.5% (to θ = 26.00°)	99.7% (to θ = 26.00°)
Refinement method	Full-matrix least-squares on F^2	Full-matrix least-squares on F^2
Data/restraints/parameters	3829/0/224	3482/0/237
Goodness-of-fit on F^2	1.063	1.084
Weights, w	$[\sigma^2(F_o^2) + (0.0361P)^2 + 0.91P]^{-1}$ $P = [\mathrm{Max}(F_o^2,0) + 2F_c^2]/3$	$[\sigma^2(F_o^2) + (0.048P)^2 + 0.32P]^{-1}$
Final R indices [$I > 2\sigma(I)$]	R_1 = 0.0420, wR_2 = 0.1154	R_1 = 0.0342, wR_2 = 0.0864
R indices (all data)	R_1 = 0.0523, wR_2 = 0.1229	R_1 = 0.0412, wR_2 = 0.0908
Largest difference in peak and hole (e Å^{-3})	2.300[a] and −0.621	0.325 and −0.610

[a] Near a positionally disordered DMSO crystallization solvent molecule.

2.3.1. Dichloro(2-formylpyridine-para-chloro-phenylhydrazone) copper(II)[Cu(H2FopClPh)Cl_2] (**1**)

Green solid. Yield: 70%. *Anal.* Calc. for $C_{13}H_{10}Cl_3CuN_3O$: C, 39.61; H, 2.56; N, 10.66. Found: C, 39.18; H, 2.11; N, 10.57%. Selected IR bands (cm^{-1}): υ(C=O) 1600 m; υ(C=N) 1598 m; υ(N=C) 1490 s; ρ(py) 629 m; υ(Cu–N) 411 m. UV–Vis (DMF, cm^{-1}): 25 550, 24 330 (shoulder) and 13 000 (broad). Molar conductivity (1 × 10^{-3} mol L^{-1}, DMF): 33.32 Ω^{-1} cm^2 mol^{-1}. Magnetic moment = 1.76 BM.

2.3.2. Chloro(2-formylpyridine-para-nitro-phenylhydrazonato) copper(II) [Cu(2FopNO_2Ph)Cl] (**2**)

Green solid. Yield: 77%. *Anal.* Calc. for $C_{13}H_9ClCuN_4O_3$: C, 42.20; H, 2.46, N, 15.21. Found: C, 42.00; H, 2.05; N, 15.36%. Selected IR bands (cm^{-1}): υ(C=N) 1607 m; υ(N=C) 1491 s; ρ(py) 649 m; υ(Cu–N) 412 m. UV–Vis (DMF, cm^{-1}): 25 510, 24 390 (shoulder) and 13 050 (broad). Molar conductivity (1 × 10^{-3} mol L^{-1}, DMF): 13.38 Ω^{-1} cm^2 mol^{-1}. Magnetic moment = 1.82 BM.

2.3.3. Dichloro(2-formylpyridine-para-chloro-phenylhydrazone) zinc(II) [Zn(H2FopClPh)Cl_2] (**3**)

White solid. Yield: 76%. *Anal.* Calc. for $C_{13}H_{10}Cl_3N_3OZn$: C, 39.43; H, 2.55; N, 10.61. Found: C, 39.34; H, 2.06; N, 10.47%. Selected IR bands (cm^{-1}): υ(NH) 3201 m; υ(C=O) 1649 s; υ(C=N) 1593 m; ρ(py) 640 m; ν(Zn–N) 408 m. ^{1}H NMR [400 MHz, DMSO-d_6, δ (ppm)]: 12.02 (s, 1H, NH); 8.63 (d, 1H, H6); 8.52 (s, 1H, H7); 7.98 [m, 4H, H3, H4, H(10,14)]; 7.63 [d, 2H, H(11,13)]; 7.51 (t, 1H, H5). ^{13}C NMR [400 MHz, DMSO-d_6, δ (ppm)]: 163.2 (C8); 151.6 (C2); 149.3 (C6); 147.1 (C7); 138.0 (C12); 137.3 (C4); 131.2 (C9); 129.8 [C(10,14)]; 128.8 [C(11,13)]; 125.3 (C5); 121.6 (C3). UV–Vis (DMF, cm^{-1}): 33 220 and 26 110. Molar conductivity (1 × 10^{-3} mol L^{-1}, DMF): 14.70 Ω^{-1} cm^2 mol^{-1}.

2.3.4. Dichloro(2-formylpyridine-para-nitro-phenylhydrazone)zinc(II) [Zn(H2FopNO_2Ph)Cl_2] (**4**)

Yellow solid. Yield: 78%. *Anal.* Calc. for $C_{13}H_{10}Cl_2N_4O_3Zn$: C, 38.41; H, 2.48; N, 13.78. Found: C, 38.42; H, 2.10; N, 13.81%. Selected IR bands (cm^{-1}): υ(NH) 3227 m; υ(C=O) 1656 s; υ (C=N) 1598 m; ρ(py) 641 m; υ(Zn–N) 409 m. ^{1}H NMR [400 MHz, DMSO-d_6, δ (ppm)]: 12.26 (s, 1H, NH); 8.64 (d, 1H, H6); 8.52 (s, 1H, H7); 8.38 [d, 2H, H(11,13)]; 8.18 [d, 2H, H(10,14)]; 7.99 (m, 2H, H3, H4); 7.51 (t, 1H, H5). ^{13}C NMR [400 MHz, DMSO-d_6, δ (ppm)]: 162.5 (C8); 151.8 (C2); 149.5 (C12); 149.3 (C7); 148.1 (C6); 138.5 (C9); 138.0 (C4); 129.4 [C(10,14)]; 125.2 (C5); 123.8 [C(11,13)]; 121.3 (C3). UV–Vis (DMF, cm^{-1}): 32 890 and 25 310. Molar conductivity (1 × 10^{-3} mol L^{-1}, DMF): 17.78 Ω^{-1} cm^2 mol^{-1}.

Crystals of the complexes were obtained from a mixture of 1:9 DMSO:acetone and were stable in the air. As shown by crystal structure determinations (see Section 3.4) in the case of the complexes with H2FopNO_2Ph one DMSO molecule attached to the metal center during the crystallization process, with release of a chloride ligand and formation of chloro(dimethylsulfoxide)(2-formylpyridine-*para*-nitrophenylhydrazonato)copper(II), [Cu(2FopNO_2Ph)- Cl (DMSO)] (**2a**) and chloro(dimethylsulfoxide)(2-formylpyridine-*para*-nitrophenylhydrazonato)zinc(II), [Zn(2FopNO_2Ph)Cl(DMSO)] (**4a**).

3. Results and discussion

Microanalyses suggest the formation of [Cu(H2FopClPh)Cl_2] (**1**), [Cu(2FopNO_2Ph)Cl] (**2**), [Zn(H2FopClPh)Cl_2] (**3**), and [Zn(H2Fop-NO_2Ph)Cl_2] (**4**). In complexes **1**, **3**, and **4** the hydrazone coordinates a neutral ligand while in **2** an anionic hydrazone is attached to the metal. The molar conductivity data reveal that the complexes are non-electrolytes, in accordance with the proposed formulations. The magnetic moments 1.76 and 1.82 BM found for complexes **1**

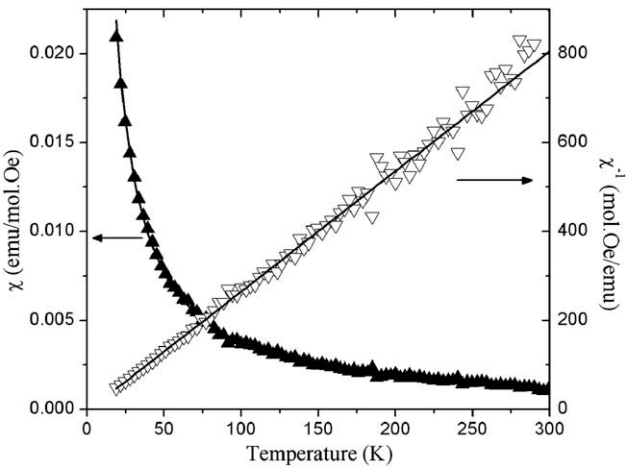

Fig. 2. Plots of magnetic susceptibilities χ and $1/\chi$ *vs T* for compound **2** in the 15–300 K temperature range. The open and full triangles represent experimental data, the curves the best least-squares fit of the data below 175 K with the Curie–Weiss law.

and **2**, respectively, at room temperature are characteristic of copper(II).

Lacking of adequate single-crystal for structural X-ray diffraction work, we explored the possibility that compound **2** could be described as penta-coordinated copper(II) in a chloro-bridged $[Cu_2(2FopNO_2Ph)_2Cl_2]$ dimeric complex. To this purpose we performed magnetic susceptibility measurements as a function of absolute temperature (T) in the 15–300 K range. The molar susceptibility $\chi(T)$ data of Fig. 2 shows a Curie–Weiss behavior that can be described by:

$$\chi(T) = \frac{N(\mu_{eff}\beta)^2}{3k(T-\vartheta)},$$

where N is the Avogadro number, β is the Bohr magneton, μ_{eff} in the effective number of magnetons per molecule, and k the Boltzman constant. Positive ϑ-values correspond to ferromagnetic (FM) exchange interaction between the unpaired Cu(II) electrons, negative ones to anti-ferromagnetic (AF) coupling. A least-squares fit of the less noisy data up to 175 K with the above equation leads to $\vartheta = 2(1)$ K and $\mu_{eff} = 1.72(1)$ BM, close to the theoretical spin-only ($S = 1/2$) value $\mu_{eff} = g\sqrt{S(S+1)} = 1.73$ $g = 2.0023$ is the free-electron gyromagnetic factor). Though the ϑ-value is zero within two standard deviation of experimental error, therefore suggesting a monomeric copper(II) complex, the possibility of an association in the lattice of two such monomers through a pair of Cu–Cl···Cu bridges with a strong intra-monomer Cu–Cl bond and a much weaker inter-monomer Cu···Cl bond can not be ruled out. In fact, feeble exchange interactions both FM and AF between the unpaired $S = 1/2$ spins of the metal ions are reported to exist in several chloro-bridged Cu(II) dimers [13–15].

3.1. Infrared spectra

The υ(C=N) vibration mode at 1592 and 1601 cm^{-1} in the spectra of the free hydrazones shifts to 1598 and 1607 cm^{-1} in the spectra of the copper(II) complexes and to 1593 and 1598 cm^{-1} in the spectra of the zinc(II) complexes, indicating coordination of the azomethine nitrogen N2 [16].

The υ(C=O) absorption at 1650–1665 cm^{-1} in the spectra of the uncomplexed hydrazones is observed at 1600–1655 cm^{-1} in those of the complexes, in accordance with coordination through the carbonyl oxygen [16,17]. In complex **2** no absorption attributable to υ(C=O) was observed, but an additional band was found at 1491 cm^{-1}, in accordance with the presence of a υ(N=C) vibration, due to the formation of a new N=C bond upon coordination with deprotonation of the hydrazone ligand [18].

The pyridine in-plane deformation mode at 618 and 619 cm^{-1} in the spectra of the hydrazones shifts to 629–649 cm^{-1} in those of the complexes, suggesting coordination of the heteroaromatic nitrogen [16,19]. Therefore, the infrared data for the complexes indicate coordination through the N_{py}–N–O chelating system.

3.2. NMR spectra

The ^1H and ^{13}C NMR assignments for the hydrazones and their zinc(II) complexes in DMSO-d_6 are reported in Sections 2.2 and 2.3. The ^1H resonances were attributed based on chemical shifts, multiplicities and coupling constants. The carbon type (C, CH) was determined by using DEPT 135 experiments. The assignments of the protonated carbons were made by 2D heteronuclear-correlated experiments (HMQC) using delay values which correspond to ^1J(C, H).

Signals from only the *E* configuration were observed for the hydrogens in the ^1H NMR spectrum of H2FopClPh. The signal at δ 12.15 was attributed to N3–H hydrogen bonded to the solvent (DMSO-d_6) [19,20]. Upon coordination to zinc(II) this signal appears at δ 12.01, suggesting that the hydrazone remains in the *E* configuration in complex **3**, to attach to the metal as a tridentate system, as confirmed by crystal structure determinations (see Section 3.4). The other hydrogen signals undergo small shifts upon coordination.

Similarly, signals from only the *E* configuration were observed for the carbons of H2FopClPh in the ^{13}C NMR spectrum. The signals at δ 148.4 and δ 162.3 were attributed to C7=N and C8=O, respectively [19,20]. These signals shift to δ 147.1 and δ 163.2, respectively in the spectrum of **3**, indicating coordination through the oxygen and the imine nitrogen. The carbons of the pyridine ring also undergo shifts upon coordination. Therefore, the NMR study clearly indicates coordination of H2FopClPh through the N_{py}–N–O chelating system.

The ^1H and ^{13}C NMR spectra of $H2FopNO_2Ph$ contain two sets of signals due to the presence of both the *E* and *Z* configurations in solution [19,20], with predominance (80%) of the *E* isomer. In fact, two signals of N3–H were observed at δ 15.83 and δ 12.33, which were attributed to the *Z* and *E* forms respectively. In the first N3–H is hydrogen bonded to the pyridine nitrogen, while in the latter it is hydrogen bonded to the solvent [19–24]. Similarly, the signals of C8=O at δ 182.9 and δ 161.8 were attributed to the *Z* and *E* isomers. The high frequency signals of N3–H and C8=O are a consequence of the presence of a N3–H···N_{py} hydrogen bond in the *Z* isomer.

Upon coordination to zinc(II) only the ^1H and ^{13}C signals due to the *E* configuration were observed. In fact, the signal of C8=O at δ 162.5, indicates that the hydrazone adopts the *E* configuration in the complex, as confirmed by crystal structure determinations. The signal of N3–H has not been observed, suggesting deprotonation in the DMSO-d_6 solution. Crystal structure determination of complex **4a**, obtained upon dissolution of **4** in 1:9 DMSO:acetone, reveals the presence of an anionic hydrazone attached to the metal center, along with one chloride and one DMSO acting as a ligand. Since in **4** a neutral hydrazone is attached to the metal along with two chloride ions, conversion of **4** into **4a** must have occurred as well in DMSO-d_6 (see Section 3.4). It is worth noticing that complex **2** also contains an anionic *para*-nitrophenyl hydrazone. Upon crystallization in 1:9 DMSO:acetone a DMSO coordinates to the metal, with formation of **2a**. Therefore we may suggest that the electron-withdrawing nitro group favors deprotonation at N3 with formation of a highly delocalized system, with the subsequent coordination of DMSO. Formation of complex **4a** from complex **4**

occurred with deprotonation at N3 followed by the release of a chloride ligand.

3.3. Electronic spectra

The $n–\pi^*$ transitions associated to the azomethine and carbonyl functions are overlapped at 33 100 cm^{-1} in the electronic spectra of the free hydrazones [16]. In the spectra of the zinc(II) complexes two absorptions attributed to these transitions were observed at ca. 33 100 cm^{-1} and 25 300–26 100 cm^{-1}. In the spectra of the copper(II) complexes the $n–\pi^*$ transitions overlap at 25 500 cm^{-1}. A new absorption at 24 400 cm^{-1} was attributed to a ligand-to-metal charge transfer transition, and a broad band at 13 000 cm^{-1} to a combination of ligand field transitions [19,25].

3.4. Structural study of [Cu(H2FopClPh)Cl_2] (**1**) [Cu(2FopNO_2Ph)Cl(DMSO)] (**2a**) [Zn(H2FopClPh)Cl_2] (**3**) and [Zn(2FopNO_2Ph)Cl(DMSO)] (**4a**)

Table 2 shows selected bond distances and angles in the crystal structures of **1**, **2a**, **3** and **4a**. Figs. 3–6 are ORTEP [26] drawings of the complexes.

Table 2
Selected bond distances (Å) and angles (°) in the molecular structures of [Cu(H2FopClPh)Cl_2] (**1**), [Cu(2FopNO_2Ph)Cl(DMSO)] (**2a**), [Zn(H2FopClPh)Cl_2] (**3**), and [Zn(2FopNO_2Ph)Cl(DMSO)] (**4a**).

Attribution	1	2a	3	4a
Bond lengths				
N1–C2	1.361(3)	1.363(3)	1.352(4)	1.348(3)
C2–C7	1.459(4)	1.459(4)	1.463(5)	1.464(3)
N2–C7	1.277(3)	1.284(3)	1.278(4)	1.278(3)
N2–N3	1.361(3)	1.363(3)	1.359(4)	1.371(3)
N3–C8	1.359(3)	1.331(3)	1.366(4)	1.337(3)
O1–C8	1.243(3)	1.285(3)	1.231(4)	1.268(3)
M–N1	2.044(2)	2.043(2)	2.182(3)	2.259(2)
M–N2	1.971(2)	1.942(2)	2.125(3)	2.059(2)
M–O1	2.137(2)	1.988(2)	2.250(2)	2.098(2)
M–Cl1	2.4344(8)		2.2337(9)	
M–Cl2	2.2212(8)		2.249(1)	
M–Cl		2.2354(7)		2.2516(7)
M–O2		2.242(2)		2.008(2)
Bond angles				
N1–C2–C7	114.4(2)	114.2(2)	114.8(3)	115.7(2)
C2–C7–N2	114.4(2)	114.8(2)	115.8(3)	117.0(2)
C7–N2–N3	124.7(2)	122.9(2)	122.4(3)	120.8(2)
N2–N3–C8	113.5(2)	107.3(2)	114.1(3)	108.3(2)
N3–C8–O1	120.4(2)	125.1(2)	120.5(3)	126.0(2)
C6–N1–M	128.6(2)	129.2(2)	126.5(2)	130.2(2)
C2–N1–M	112.4(2)	112.3(2)	114.8(2)	111.6(2)
C7–N2–M	118.5(2)	118.6(2)	119.3(2)	120.5(2)
N3–N2–M	116.8(2)	118.5(2)	118.0(2)	118.7(1)
C8–O1–M	112.0(2)	110.6(2)	115.2(2)	112.1(2)
N1–M–N2	78.91(9)	79.86(9)	73.9(1)	74.95(7)
N2–M–O1	76.17(8)	78.52(8)	71.30(9)	74.90(7)
N1–M–O1	150.28 (8)	158.06(8)	143.18(9)	149.56(7)
N1–M–Cl1	105.26(7)		98.75(8)	
N1–M–Cl2	97.71(7)		103.48(8)	
N2–M–Cl1	92.90(7)		135.35(8)	
N2–M–Cl2	163.28(7)		108.07(8)	
O1–M–Cl1	92.00(6)		97.65(7)	
O1–M–Cl2	101.48(6)		98.27(8)	
Cl1–M–Cl2	103.76(3)		116.39(4)	
N1–M–Cl		98.88(6)		98.89(5)
N1–M–O2		93.78(8)		98.26(7)
N2–M–Cl		162.64(7)		134.73(6)
N2–M–O2		95.06(8)		117.62(8)
O1–M–Cl		100.63(5)		105.19(6)
O1–M–O2		91.80(7)		91.98(7)
O2–M–Cl		102.29(5)		107.65(5)

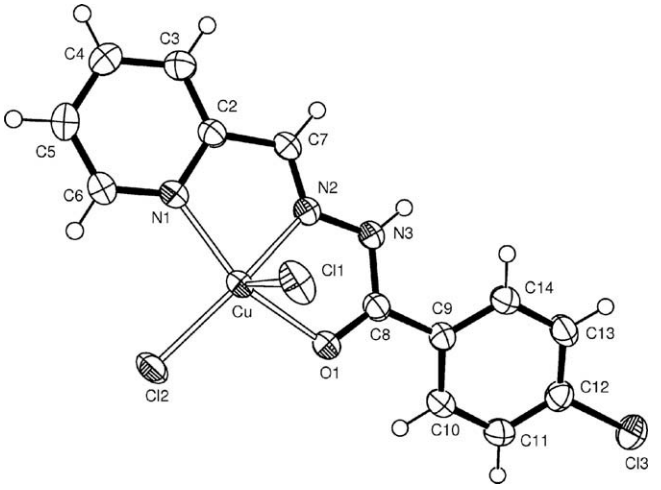

Fig. 3. Molecular plot of [Cu(H2FopClPh)Cl_2] (**1**) showing the labeling of the non-H atoms and their displacement parameters at the 50% probability level. Metal–ligand interactions are indicated by open bonds.

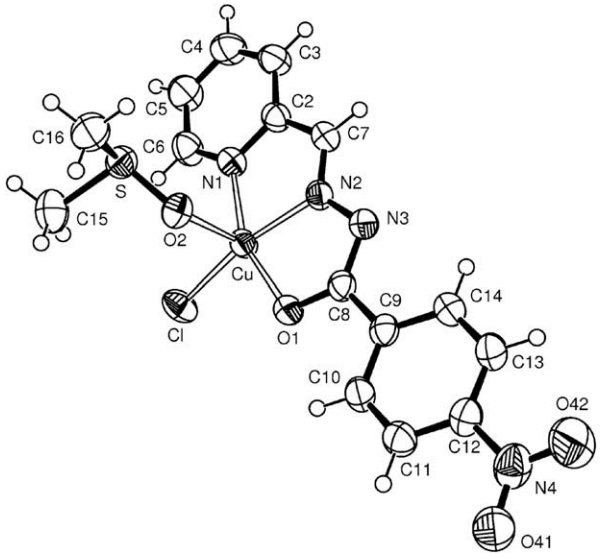

Fig. 4. Molecular plot of [Cu(2FopNO_2Ph)Cl(DMSO)] (**2a**).

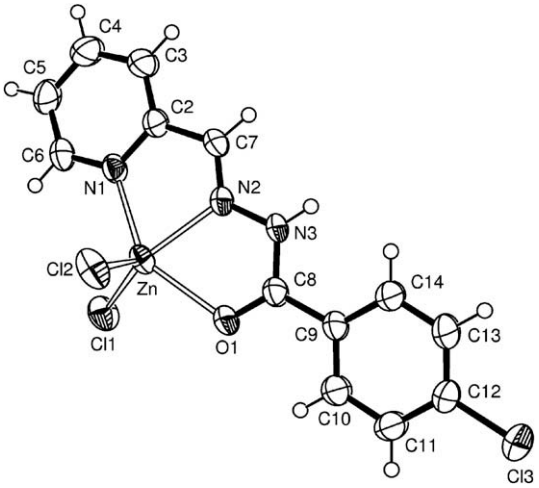

Fig. 5. Molecular plot of [Zn(H2FopClPh)Cl_2] (**3**).

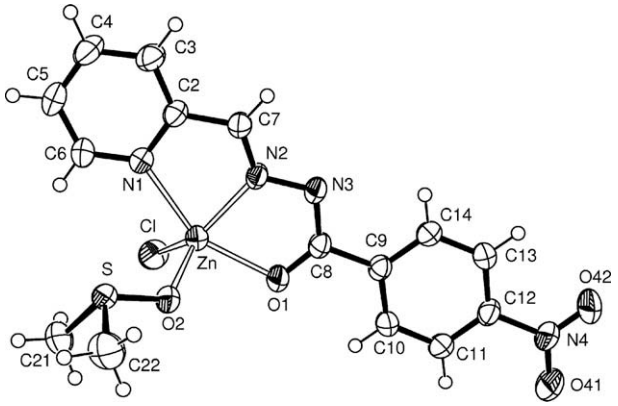

Fig. 6. Molecular plot of [Zn(2FopNO$_2$Ph)Cl(DMSO)] (**4a**).

The copper(II) and zinc(II) ions present coordination number five, and are attached to a hydrazone molecule acting as a tridentate ligand through the pyridine and imine nitrogens, and the carbonyl oxygen. Two chloride ions occupy the remaining coordination positions in the complexes with H2FopClPh. In the complexes with H2FopNO$_2$Ph one chloride and one O-bonded DMSO are attached to the metal, along with an anionic hydrazone.

In all compounds, the hydrazone Pyr(C=N)N(C=O)N skeletal fragment defines the coordination plane [rms deviation of atoms from the least-squares plane less than 0.040 Å] with the metal ion laying closer onto this plane in complexes **2a** and **4a** than in complexes **1** and **3** [Cu(II) ions at 0.382(2) and 0.104(1) Å in **1** and **2a** and Zn(II) ions at 0.358(2) and 0.105(2) Å in **3** and **4a**, respectively]. In **2a** and **4a** a competition between one chloride ion and the anionic hydrazone for the positively charged metal probably occurs. The interaction between the metal center and the anionic hydrazone results in the metal laying closer to the hydrazone skeleton plane in **2a** and **4a** than in **1** and **3**, where the attraction effect of two chloride ions for the positive metal center predominates over the interaction between the metal and a neutral hydrazone. The phenyl ring and the coordination plane in complexes **1**, **2a**, **3** and **4a** subtend dihedral angles of 22.0(1), 9.5(1), 9.5(2), and 2.5(1)°. In **2a** and **4a** the terminal NO_2 group is nearly coplanar with the phenyl ring [angled at 7.1(5) and 0.2(6)°, respectively].

For complexes **1** and **3** the hydrazone C8–O1 bond distances are 1.243(3) and 1.231(4) Å, respectively, while in complexes **2a** and **4a** the C8–O1 bond distances are 1.285(3) and 1.268(3) Å respectively, in accordance with a higher single bond character for the latter which present an anionic hydrazone ligand. Similarly, the N3–C8 bond distances are 1.359(3) and 1.366(4) Å for **1** and **3** respectively and 1.331(3) and 1.337(3) Å for **2a** and **4a** respectively, in agreement with a higher double bond character in the latter. Interestingly, the O1–M bond distances are 2.137(2) and 2.250(2) Å for **1** and **3** and 1.988(2) and 2.098(2) Å for **2a** and **4a**, in accordance with the presence of a negative charge at the oxygen in the latter, which increases the strength of the M–O1 bond.

In going from complexes **1** and **3** to complexes **2a** and **4a** the N1–M–N2 and N2–M–O1 angles undergo small changes (ca. 1–3°, see Table 2); the N1–M–O1 changes from 150.28(8) and 143.18(9)° in **1** and **3**, respectively, to 158.06(8) and 149.56(7)° in **2a** and **4a** due to higher delocalization in the latter and to the change of the N3 hybridization from sp^3 to sp^2. Similarly the N3–C8–O1 angles goes from 120.4(2) and 120.5(3)° in **1** and **3** to 125.1(2) and 126.0(2)° in **2a** and **4a** due to the same effect.

Comparison between **1** and **3** and between **2a** and **4a** reveals that the bond distances within the hydrazone ligand are not very different but, as expected, the M–L [M = Cu(II), Zn(II)] distance varies appreciably with the metal ion. Similarly, the bond angles within the hydrazone backbone do not change significantly but the angles around the metal undergo appreciable variations upon changing the metal center.

The crystallization DMSO solvent molecule in crystals **1** and **3** acts as acceptor of a N3–H···O bond [N3···O length and N3–H···O angle of 2.685 Å and 149.6° for **1** and 2.706 Å and 161.6° for **3**].

4. Conclusions

2-Formylpyridine-*para*-cholro-phenyl-hydrazone (H2FopClPh) and 2-formylpyridine-*para*-nitro-phenyl-hydrazone (H2FopNO$_2$Ph) react with copper chloride and with zinc chloride with formation of [Cu(H2FopClPh)Cl$_2$] (**1**), [Cu(2FopNO$_2$Ph)Cl] (**2**), [Zn(H2FopClPh)Cl$_2$] (**3**) and [Zn(H2FopNO$_2$Ph)Cl$_2$] (**4**), in which the hydrazones coordinate to the metal center as N$_{py}$–N–O chelating systems. Upon crystallization in DMSO:acetone conversion of **2** into [Cu(2FopNO$_2$Ph)Cl(DMSO)] (**2a**) and of **4** into [Zn(2FopNO$_2$Ph)Cl(DMSO)] (**4a**) occurs. In the case of **2a** the coordinating ability of DMSO leads to its attachment to the metal center with expansion of the metal coordination number. The electron-withdrawing effect of the *para*-nitro group probably makes the metal center more positive and more able to accept the fifth ligand. In the case of **4a** the electron-withdrawing effect of the *para*-nitro group favors deprotonation at N3, with release of HCl, and attachment of a DMSO molecule to the metal. Interestingly, as we showed in a previous work, crystallization of [Zn(H2BzpNO$_2$Ph)Cl$_2$] (H2BzpNO$_2$Ph = 2-benzoylpyridine-*para*-nitro-phenyl-hydrazone) in DMSO:acetone lead to the formation of [Zn(2BzpNO$_2$Ph)Cl(DMSO)], also promoted by the presence of the *para*-nitro group [20].

Supplementary data

CCDC 714806, 714807, 714808, and 714809 contain the supplementary crystallographic data for complexes **1**, **2a**, **3** and **4a**. These data can be obtained free of charge via http://www.ccdc.cam.ac.uk/conts/retrieving.html, or from the Cambridge Crystallographic Data Centre, 12 Union Road, Cambridge CB2 1EZ, UK; fax: (+44) 1223-336-033; or e-mail: deposit@ccdc.cam.ac.uk.

Acknowledgements

The authors are grateful to Capes and CNPq (Brasil) and to CONICET (Argentina) for financial support. O.E.P. is a research fellow of CONICET, Argentina.

References

[1] S. Rollas, Ş.G. Küçükgüzel, Molecules 12 (2007) 1910 (and references therein).
[2] P. Vicini, M. Incerti, I.A. Doytchinova, P. La Colla, B. Busonera, R. Loddo, Eur. J. Med. Chem. 41 (2006) 624 (and referentes therein).
[3] H.J.C. Bezerra-Netto, D.I. Lacerda, A.L.P. Miranda, H.M. Alves, E.J. Barreiro, C.A.M. Fraga, Bioorg. Méd. Chem. 4 (2006) 7924 (and references therein).
[4] O. Pouralimardan, A.-C. Chamayou, C. Janiak, H. Hosseini-Monfared, Inorg. Chim. Acta 360 (2007) 1599.
[5] C. Basu, S. Chowdhury, R. Banerjee, H.S. Evans, S. Mukherjee, Polyhedron 26 (2007) 3617.
[6] M. Bakir, O. Green, W.H. Mulder, J. Mol. Struct. 873 (2008) 17.
[7] J.L. Buss, J. Neuzil, P. Ponka, Biochem. Soc. Trans. 30 (2002) 755.
[8] Enraf-Nonius (1997–2000), COLLECT, Nonius BV, Delft, The Netherlands.
[9] Z. Otwinowski, W. Minor, in: C.W. Carter Jr., R.M. Sweet (Eds.), Methods in Enzymology, vol. 2, Academic Press, New York, 1997, p. 307.
[10] A.L. Spek, PLATON, A Multipurpose Crystallographic Tool, Utrecht University, Utrecht, The Netherlands, 1998.
[11] G.M. Sheldrick. SHELXS-97. Program for Crystal Structure Resolution, University of Göttingen, Göttingen, Germany, 1997.
[12] G.M. Sheldrick. SHELXL-97, Program for Crystal Structures Analysis,University of Göttingen, Göttingen, Germany, 1997.
[13] W.E. Marsh, W.E. Hatfield, D.J. Hodgson, Inorg. Chem. 21 (1982) 2679.

[14] W.E. Marsh, K.C. Patel, W.E. Hatfield, D.J. Hodgson, Inorg. Chem. 22 (1983) 511.
[15] S. Mandal, F. Lloret, R. Mukherjee, Inorg. Chim. Acta 362 (2009) 27.
[16] A. Perez-Rebolledo, O.E. Piro, E.E. Castellano, L.R. Teixeira, A.A. Batista, H. Beraldo, J. Mol. Struct. 794 (2006) 18.
[17] K. Nakamoto, Infrared and Raman Spectra of Inorganic and Coordination Compounds, fourth ed., Wiley, New York, 1986.
[18] P.B. Sreeja, M.R. Prathapachandra Kurup, A. Kishore, C. Jasmin, Polyhedron 23 (2004) 575.
[19] A.A. Recio Despaigne, J.G. Da Silva, A.C.M. Do Carmo, O.E. Piro, E.E. Castellano, H. Beraldo, J. Mol. Struct. 920 (2009) 97.
[20] A.A. Recio Despaigne, J.G. Da Silva, A.C.M. Do Carmo, O.E. Piro, E.E. Castellano, H. Beraldo, Inorg. Chim. Acta 362 (7) (2008) 2122.
[21] A.P. Rebolledo, M. Vieites, D. Gambino, O.E. Piro, E.E. Castellano, C.L. Zani, E.M. Souza-Fagundes, L.R. Teixeira, A.A. Batista, H. Beraldo, J. Inorg. Biochem. 99 (2005) 698.
[22] A.M.B. Bastos, A.F.C. Alcântara, H. Beraldo, Tetrahedron 61 (2005) 7045.
[23] A. Pérez-Rebolledo, G.M. de Lima, N.L. Speziali, O.E. Piro, E.E. Castellano, J.D. Ardisson, H. Beraldo, J. Organomet. Chem. 691 (2006) 3919.
[24] A.P. Rebolledo, G.M. de Lima, L.N. Gambi, N.L. Speziali, D.F. D.F.Maia, C.B. Pinheiro, J.D. Ardisson, M.E. Cortés, H. Beraldo, Appl. Organomet. Chem. 17 (2003) 945.
[25] I.C. Mendes, J.P. Moreira, A.S. Mangrich, S.P. Balena, B.L. Rodrigues, H. Beraldo, Polyhedron 26 (13) (2007) 3263.
[26] C.K. Johnson, ORTEP-II. A Fortran Thermal-Ellipsoid Plot Program. Report ORNL-5318, Oak Ridge National Laboratory, Tennessee, USA, 1976.